Local spin-density theory of itinerant magnetism in crystalline and amorphous transition metal alloys



1992 J. Phys.: Condens. Matter 4 7257

(http://iopscience.iop.org/0953-8984/4/35/010)

J. Phys.: Condens. Matter 4 (1992) 7257–7284. Printed in the UK

# Local spin-density theory of itinerant magnetism in crystalline and amorphous transition metal alloys

I Turek†, Ch Becker, and J Hafner

Institut für Theoretische Physik, Technische Universität Wien, Wiedner Hauptstraße 8-10, A-1040 Wien, Austria

Received 10 March 1992, in final form 19 May 1992

**Abstract.** We present self-consistent spin-polarized electronic structure calculations for realistic models of amorphous transition metal alloys. The atomic structure is prepared by a simulated molecular-dynamic quench, based on interatomic forces calculated using hybridized nearly-free-electron tight-binding-bond theory. The electronic structure is calculated in the local spin-density approximation, using a linear muffin-tin orbital (LMTO) supercell approach. Detailed results for crystalline and amorphous alloys of Ni, Co and Fe with Zr are presented. $Ni_xZr_{1-x}$ alloys are predicted to be paramagnetic for $x \leqslant 0.85$, both in the crystalline and in the amorphous state. In $Co_xZr_{1-x}$ the onset of magnetic ordering occurs at $x \simeq 0.67$ for crystalline and at $x \simeq 0.50$ for amorphous alloys. The Co-rich alloys are predicted to be strong ferrimagnets. The formation of the negative Zr moments is related to a covalent coupling of Co- and Zr-d states, which is strongest for the Co minority-spin states. The enhancement of magnetism in the glassy alloys is related to an increase of the density of states at the Fermi level induced by structural disorder. In both crystalline and amorphous $Fe_xZr_{1-x}$ alloys, the onset of ferrimagnetic ordering occurs at $x \simeq 0.33$. In contrast to the Co-based alloys, $Fe_xZr_{1-x}$ alloys are weak magnets. For $x \geqslant 0.75$ the competition between ferromagnetic and antiferromagnetic exchange interactions leads to the formation of negative moments on isolated Fe sites. The number of negative Fe moments increases strongly for $x \geqslant 0.90$, leading to a decrease of the average moment in the Fe-rich limit. We show that the formation of negative local Fe moments is related to a large number of contracted Fe–Fe pairs. The predictions of local spin-density theory are found to be in excellent agreement with experiment. For all crystalline and amorphous alloys the local exchange splitting of the 3d states is shown to be correlated linearly with the local magnetic moment, with a slope of $\simeq 1$ eV$\mu_B^{-1}$. This relation holds for all types of magnetic order and also for the crystalline and amorphous pure metals.

## 1. Introduction

For the crystalline intermetallic compounds formed by two transition metals, local spin-density (LSD) theory has made important contributions towards a fundamental understanding of the electronic and magnetic properties [1–5]. The physical mechanism for the formation of magnetic moments and for the variation of magnetization with composition and density is now quite well understood. On the

† On leave of absence from Institute of Physical Metallurgy, Czechoslovak Academy of Sciences, Žižkova 22, CS-61662 Brno, Czechoslovakia.

0953-8984/92/357257+28$04.50  

other hand, many of the interesting magnetic properties of amorphous transition-metal alloys remain a challenge to the band theory of magnetism. The difficulties begin at a disconcertingly low level, namely with the magnetic properties of the hypothetic amorphous forms of pure Fe and Co. Whereas the data for nominally pure amorphous Co [6,7] and the extrapolation of the magnetization data of dilute alloys [8] point to a magnetic moment which is about as large as for crystalline Co, Grigson *et al* [9] report a very low moment of $\mu \simeq 0.35\mu_B$ for nominally pure amorphous Fe. This value is supported roughly by data on amorphous Fe with dilute impurities [10]. The situation becomes even more complex on alloying with an 'early' transition metal $E$ ($E$ = Sc, Ti, V, Y, Zr, Nb): in contrast to the amorphous Co alloys which become less magnetic on addition of $E$ atoms, amorphous Fe alloys become more magnetic, at least initially, as $E$ atoms are added [8]. For most amorphous Co alloys, the available information is consistent with moderately strong ferromagnetism. Amorphous Fe alloys show strong local-environment effects and strong thermal expansion anomalies (Invar effect) over a large composition range, taken as an indication of weak magnetism. Neutron diffraction data [11] on amorphous $Fe_xZr_{1-x}$ and $Fe_xY_{1-x}$ alloys point to an antiferromagnetic Zr (Y) contribution to the net magnetization. Fe-rich glassy alloys ($x \geqslant 0.85$ for $Fe_xZr_{1-x}$, $x \geqslant 0.5$ for $Fe_xY_{1-x}$) have non-collinear spin-structures, but there is a lasting controversy whether these alloys (and pure amorphous iron) should be considered as genuine spin glasses (i.e. with an isotropic distribution of the directions of the moments and a vanishing average moment) or as asperomagnets (i.e. with randomly frozen transverse components and a non-vanishing net moment) [12–15].

The reason for the slow progress in the band theory of amorphous magnetism is twofold. (i) Even if relaxed dense random packing (DRP) models yield a tolerably realistic first approximation to the structure of the pure amorphous metals, the glassy alloys are characterized by strong chemical and topological short-range-order effects [16–18]. The construction of realistic structural models requires accurate interatomic potentials and efficient dynamical modelling algorithms. (ii) The combined evidence for strong structural and magnetic fluctuations suggests that spin-polarized calculations should achieve local self-consistency between potential and charge distribution on every atomic site. Most spin-polarized electronic structure calculations for amorphous magnets are based on parametrized tight-binding (TB) Hamiltonians with fixed transfer integrals. They are either non-self-consistent [19,20] or achieve self-consistency only within the restricted framework of a TB calculation with a fixed site-independent Hubbard-type intra-atomic Coulomb interaction [21].

Recently, some progress has been achieved in both areas. It has been shown that for disordered transition-metal alloys the strong covalent d-bond forces may be cast into the form of a pair interaction via a tight-binding bond (TBB) approach [22–26]. The corresponding pair potentials are of a rather unusual form, being strongly non-additive with a preference for strong and short unlike-atom bonds. The non-additivity increases with the difference in the transition-metal valence. These potentials yield partial correlation functions in full agreement with the best structure determinations using neutron diffraction and isotopic substitution [26–28].

For the calculation of the electronic spectrum of amorphous and liquid systems it has been shown that a locally self-consistent calculation can be performed in a supercell approximation [29], modelling the glass by a small ensemble of atoms in a periodically repeated supercell. Using efficient band-structure codes such as the linear muffin-tin orbital (LMTO) method [30,31] supercell calculations for up to 60–

80 atoms per cell are now feasible. These calculations yield reliable results for the electronic spectrum of liquid [32,33] and glassy [34,35] metals in good agreement with the available photoemission, x-ray and Auger spectra. The convergence of the supercell method with respect to the number of atoms in the cell may be checked by transforming the LMTO Hamiltonian to a canonical tight-binding form [36] and calculating the electronic spectrum of a large system ($N \geqslant 1000$ atoms) by a real-space recursion technique [37]. By comparing the results of supercell and recursion calculations for a fixed crystal potential, it may be shown that the supercell approach is not seriously affected by the periodic boundary conditions [38].

We have recently used the spin-polarized LMTO supercell approach to investigate the electronic and magnetic structure of amorphous Fe and Co as a function of density [39]. For the variation of the average magnetic moment with density, our results are in good agreement with calculations on the basis of a TB-Hubbard Hamiltonian [21,40], but substantial differences appear on a local level. The TB calculations predict that at low densities amorphous Fe is a strong inhomogeneous ferromagnet and that an increasing density leads to a reduction of the average magnetic moment and a broadening of the distribution of the moments. The locally self-consistent LSD calculation predicts low-density amorphous iron to be an inhomogeneous ferromagnet, but under compression the magnetic polarization acquires an antiferromagnetic component. An increasing number of sites have a large negative moment, so that the distribution of the magnetic moments is bimodal with very few non-magnetic sites. Under further compression the distributions of both positive and negative moments are broadened and shifted to lower values. Under high compression, the distribution of the magnetic moments is that corresponding to an Ising spin-glass. Amorphous cobalt, on the other hand, remains an inhomogeneous ferromagnet up to rather high density and shows a smooth transition to a non-magnetic state under very high compression.

In the present paper we have extended the self-consistent spin-polarized LSD calculations to crystalline and amorphous Fe–Zr, Co–Zr and Ni–Zr alloys. Realistic structure models have been constructed using molecular dynamics simulations on the basis of hybridized nearly-free-electron tight-binding-bond (NFE-TBB) potentials. $Ni_xZr_{1-x}$ alloys are predicted to be paramagnetic at all concentrations covered in our study. Amorphous $Co_xZr_{1-x}$ alloys are predicted to be ferrimagnetic for $x \geqslant 0.50$, the formation of the negative moments on the Zr-sites is due to a covalent coupling of the Zr-d states to the Co-d states. The crystalline Laves phase $Co_2Zr$ is found to be at the margin between paramagnetism and ferrimagnetism—in agreement with experiment. Thus in Co–Zr amorphicity is predicted to enhance magnetism. This differs from the behaviour of the Fe–Zr alloys, where the onset of magnetic order occurs at the same composition for the glassy alloys and the crystalline intermetallic compounds. In the Fe-rich amorphous phases, the magnetic polarization of the iron atoms acquires a substantial antiferromagnetic component, as in pure amorphous iron. The analysis of the electronic density of states points to strong magnetism in Co–Zr and weak magnetism in Fe–Zr. We show that the local fluctuations are strongly coupled to fluctuations in the spin-dependent potential. There exists a universal proportionality between the local magnetic moment and the local exchange splitting. The value of 1 $eV\mu_B^{-1}$ for this ratio is the same as that resulting from our LSD calculations for amorphous Co and Fe. Very recently Himpsel [41] suggested on the basis of an analysis of photoemission and inverse photoemission data that this proportionality holds for all magnetic systems; our results show that it holds even on a local level.

## 2. Structural modelling

The simulation of the amorphous structures for Ni–Zr and Fe–Zr alloys on the basis of quantum pair and volume forces has been described in detail in our previous papers [18,26,27]. The main limitation of the supercell method is of course the small number of atoms per supercell ($N \leqslant 80$) that can be handled even with the most efficient band-structure techniques and the limited number of configurations that can be considered in a configuration average. In order to select representative models we proceed in the following way. Two molecular dynamics simulations are performed in parallel, one for ensembles that are sufficiently large to allow for a critical comparison of the calculated correlation functions and structure factors with diffraction data (typically $N = 1000$–$2000$) and one for small ensembles with $N = 64$ that prepares the coordinates for the supercell calculations. The configurations for which the electronic structures are calculated are chosen such that the partial correlation functions calculated for a single 64-atom configuration are as close as possible to the correlation functions obtained from an extended configuration average over the large ensemble. As an example we show in figure 1 the partial correlation functions for amorphous $Co_{67}Zr_{33}$. We see that the supercell correlation functions reproduce all significant details of the amorphous structure. We also find that the interatomic distances and partial coordination numbers correspond very closely to those in the Laves phase $Co_2Zr$. For a more detailed discussion of the local order in Fe–Zr and Ni–Zr glasses, we refer to [18,27]. Here we only stress that in all (Fe, Co, Ni)–Zr glasses we find a trend from a trigonal-prismatic to a polytetrahedral local topology and from moderate to strong chemical order with decreasing Zr content. The tendency towards ordering increases in the sequence Fe–Zr, Co–Zr, Ni–Zr. The trend in amorphous structures reflects the trends in the structure of the crystalline phases, where we find trigonal-prismatic phases in the Zr-rich and polytetrahedrally close-packed phases in the Fe-, Co-, Ni-rich range of the phase diagram [42], see table 1.

**Table 1.** Crystal structures of the Fe–Zr, Co–Zr and Ni–Zr compounds. Compiled after Villars and Calvert [42]. Boldface: trigonal-prismatic structures. Italics: polytetrahedral close-packed structures.

| X | Fe | Co | Ni |
|---|---|---|---|
| $XZr_3$ | **$BRe_3$** | **$BRe_3$** | **$CFe_3$** |
| $XZr_2$ | **$CuAl_2$** | **$CuAl_2$** | **$CuAl_2$** |
| XZr | — | CsCl | **BCr** |
| $X_2Zr$ | *$Cu_2Mg$* | *$Cu_2Mg$* | *$Cu_2Mg$* |
| $X_3Zr$ | — | — | $Ni_3Sn$ |
| $X_{23}Zr_6$ | *$Mn_{23}Th_6$* | *$Mn_{23}Th_6$* | — |
| $X_5Zr$ | — | — | *$Be_5Au$* |

## 3. Spin-polarized electronic structure calculations

We have adopted the scalar relativistic linear muffin-tin orbital method in the atomic-sphere approximation (LMTO-ASA) [30,31] for the spin-polarized electronic structure

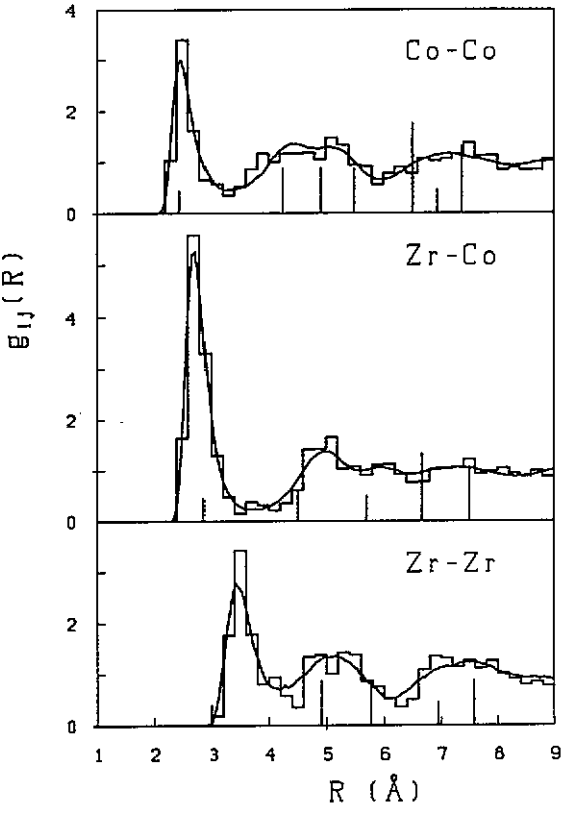


**Figure 1.** Partial pair correlation functions for amorphous $Co_{67}Zr_{33}$. The full curves show the results of a simulated molecular dynamics quench for a $N = 1372$ atoms model and an extended ensemble average at room temperature. The histogram shows the pair correlations for a single $N = 64$ atom configuration used in the electronic structure calculations. The vertical bars mark the nearest-neighbours distances in the Laves phase $Co_2Zr$.

calculations. Exchange and correlation are described in the local spin density (LSD) approximation [43] with the von Barth–Hedin [44] parametrization of the exchange-correlation functional. For crystalline $Co_2Zr$, which is very close to the onset of ferromagnetism, the influence of the precise form of the exchange-correlation functional has been tested in detail. For the crystalline phases, the Brillouin-zone integrations have been performed using the linear tetrahedron-method with up to 505 $k$-points.

The supercells representing the amorphous alloys have the translational periodicity of a simple cubic lattice, but not its point-group symmetry. For the determination of the density of states (DOS), we used only the eigenvalues at the special point $k = (0.5, 0.5, 0.5)\pi/a$ and obtained a smooth DOS by a Gaussian broadening, the Gaussians having a FWHM of 0.2 eV. For the relatively narrow d bands with a high DOS this is an acceptable approximation. The structures appearing in some cases at the lower edge of the band result from a few low-lying sp states arising fom particular local configurations. If we could proceed to a more extended configuration average, these structures would average out to form a smooth band tail. The main part of the d band however would hardly be affected by a more extended averaging. The high computational cost of an extended sampling seems not to be justified for the mere smoothening of a band tail. The precise form of the band tail does not influence any of the physical properties considered here.

In the LMTO method, the Schrödinger equation for an electron wavefunction $u_{RL}$

within the atomic sphere centred at the site $\boldsymbol{R}$ may be formulated as [30]

$$\sum_{R'L'} [P_{RL}(E)\,\delta_{RL,R'L'} - S_{RL,R'L'}]\, N^{-1}_{R'L'}(E)\, u_{R'L'} = 0 \tag{1}$$

where $S$ is a structure-constant matrix and $P$ a diagonal potential function matrix ($N$ is a normalization function, $L$ stands for the set of principal, angular momentum, magnetic and spin quantum numbers, $L \hat{=} nlm\sigma$). A conventional parametrization of the potential function is

$$P_{RL}(E) = \left(\frac{W_{RL}}{E - C_{RL}} + \gamma_{RL}\right)^{-1} \tag{2}$$

with the potential parameters $C_{RL}$, $W_{RL}$, $\gamma_{RL}$ describing the centre, width and distortion of the pure $RL$ band. With this parametrization, the exchange splitting $\Delta_R$ of the atom at site $\boldsymbol{R}$ is given by $\Delta_R = C_{Rnlm\downarrow} - C_{Rnlm\uparrow}$, where $nl = 3d$ for Fe, Co, Ni and $nl = 4d$ for Zr.

In the supercell approach the local potential parameters are determined self-consistently. This is very important for exploring the correlation between local fluctuations in the potential and in the magnetic moment. This correlation is necessarily obscured in calculations treating self-consistency only in an approximate way. In our supercell calculations, the iteration procedure was stopped after the total magnetic moment per atom converged within $10^{-4}\mu_B$ and the local moments converged within 0.01 $\mu_B$.

In the following we present our results for the electronic and magnetic properties of the crystalline and amorphous Fe–Zr, Co–Zr and Ni–Zr alloys.

## 4. Electronic and magnetic structure

### *4.1. Ni–Zr alloys*

A preliminary account of non-spin-polarized electronic structure calculations for some crystalline and amorphous Ni–Zr alloys has already been published [34]. Here we report on spin-polarized calculations on an extended series of alloys in the Ni-rich range. The crystallographic data for the two Ni-rich crystalline compounds covered in our study are summarized in table 2. This table also contains the information on the ratio of the atomic sphere radii and the $k$-space grid for the Brillouin-zone integrations. Figure 2 shows the DOS for the paramagnetic state of $Ni_3Zr$ ($Ni_3Sn$ type) and $Ni_5Zr$ ($AuBe_5$ type). Results for $NiZr_2$ ($CuAl_2$ type), NiZr (CrB type) and $Ni_2Zr$ ($Cu_2Mg$ type) have been reported by Jank *et al* [34]. The paramagnetic state is found to be the magnetic ground state for all these compounds. This is in accordance with the Stoner theory of itinerant magnetism: at all compositions the Ni DOS at the Fermi level is substantially lower than the critical value of 2 states $eV^{-1}$ $atom^{-1}$.

The calculated DOS suggests a strong covalent interaction between Ni-d and Zr-d states. The Ni states are concentrated at the bottom of the valence band, with increasing Zr concentration the centre of gravity of the Ni band is shifted to higher bonding energies. In the Ni-rich alloys a pseudogap separates the Ni-dominated low-lying band from the Zr-dominated states at higher energy. In $Ni_5Zr$ the empty

**Table 2.** Crystallographic data of Ni-rich Ni–Zr intermetallic compounds, Wigner–Seitz radii, number of $k$-points for Brillouin-zone integration.

| Phase | Pearson symbol | Lattice constant ($nm$) | $R_{Zr}/R_{Ni}$ | Number of $k$-points |
|---|---|---|---|---|
| $Ni_3Zr$ | hP8 | $a = 0.5309$<br>$c = 0.43034$ | 1.225 | 396(112) |
| $Ni_5Zr$ | cF24 | $a = 0.6702$ | 1.225 | 240 |

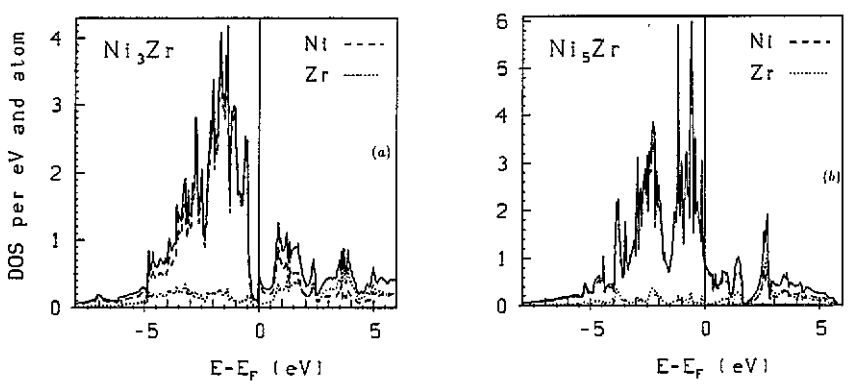


**Figure 2.** Total and site-decomposed electronic density of states for the crystalline intermetallic compounds $Ni_3Zr$ ($Ni_3Sn$ type) ($a$) and $Ni_5Zr$ ($AuBe_5$ type) ($b$). Full curve, total DOS; broken curve, Ni-DOS; dotted curve, Zr DOS.

Zr band has the character of an impurity band. At lower Ni concentrations the DOS minimum is shifted below the Fermi energy. The pseudogap in the electronic DOS reflects the pronounced chemical short-range order: in all crystalline Ni–Zr compounds there is a preference for heterocoordination.

The electronic DOS of amorphous $Ni_{85}Zr_{15}$ alloy (figure 3) and of the remaining Ni–Zr amorphous alloys (presented in [34]) is very similar to that of the crystalline intermetallic compounds. The DOS of $a$-$Ni_{85}Zr_{15}$ shows the strong bonding–antibonding splitting of the Ni-d band (with peaks 0.5 and 2.5 eV below $E_F$) and the strong Zr peak about 2.7 eV above the Fermi level. With increasing Zr content the bonding–antibonding splitting is reduced and the Ni-d band acquires a more triangular form, as in crystalline $Ni_3Zr$ and NiZr. At a Zr content beyond 50%, a DOS minimum appears just below the Fermi energy, as in the corresponding crystalline compounds.

The electronic structure of crystalline and amorphous Ni–Zr alloys has been investigated by Amamou *et al* [45,46] using photoemission spectroscopy, susceptibility and specific heat measurements; photoemission data for the amorphous alloys have also been published by Oelhafen [47]. The photoemission intensity is an average over the local angular-momentum decomposed densities of states, weighted with the $l$-dependent photoionization cross sections. Starting from the self-consistent LMTO-potentials, the photoionization cross sections may be calculated in a single-scatterer final-state approximation and completely neglecting wavevector conservation [48–50]. For crystalline materials, the last approximation is justified only for the high excitation energies of x-ray photoemission spectroscopy (XPS) where wavevector

conservation is relaxed by phonon broadening. For amorphous alloys where the wavevector is not a conserved quantity, the approach may be extended to the much lower excitation energies of ultraviolet photoemission spectroscopy (UPS). The variation of the photoionization cross section with the energy of the incident photon allows to assess the detailed validity of the calculated DOS in a combined UPS-XPS experiment. Figure 4 compares the calculated photoelectron spectra with the experimental results of Amamou [45] and Oelhafen [47]. Altogether we find that the theoretical predictions are confirmed, except for a slight overestimate of the depth of the DOS minimum just below $E_F$. As a consequence, the Fermi energy is shifted upwards and the distance between $E_F$ and the main peak of the d band is increased. This seems to indicate that the calculated structure slightly overestimates the tendency towards chemical ordering. Our analysis of the atomic structure had shown that if there is any difference at all between the neutron-diffraction data and the simulation results, it is a slightly larger amplitude of the concentration fluctuations in the model structure.

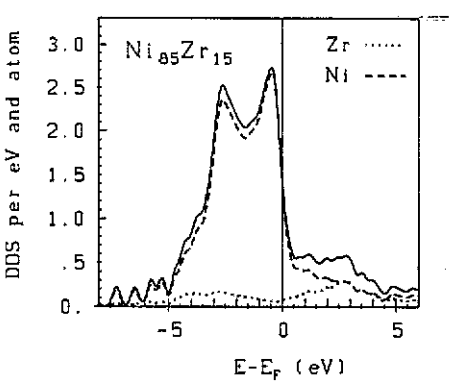


**Figure 3.** Total and site-decomposed electronic density of states for amorphous $Ni_{85}Zr_{15}$. For key, see figure 2.

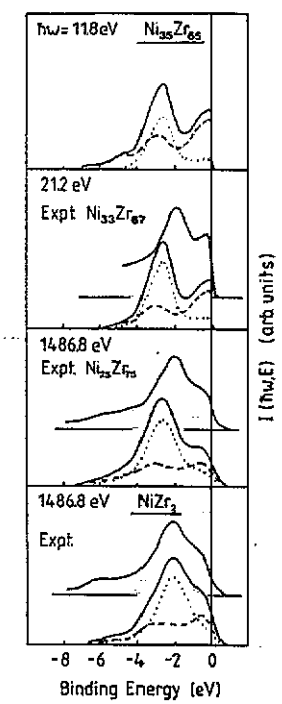


**Figure 4.** Photoemission intensities of crystalline $NiZr_2$ and amorphous $Ni_{35}Zr_{65}$. The full curves represent the total photoemission intensity, the dotted and broken curves the Ni and Zr contributions. The experimental data are from Amamou [45] and Oelhafen [47].

It is difficult to extract the DOS at the Fermi level from the susceptibility and specific heat measurement. The specific heat DOS is larger than the bare DOS by a mass enhancement factor $(1 + \lambda_{ep} + \lambda_{sf})$ arising from electron–phonon coupling

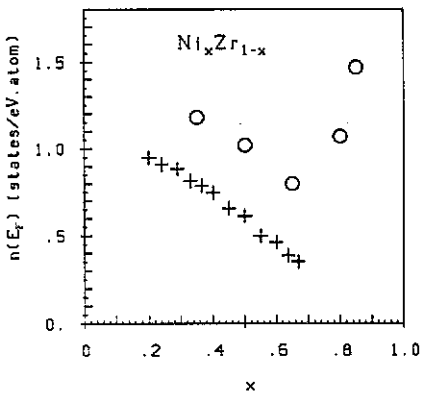


**Figure 5.** Electronic density of states at the Fermi energy in glassy Ni–Zr alloys: crosses, experimental estimate of Altounian and Ström-Olsen [51]; circles, present results (see text).

and spin fluctuations, the susceptibility DOS differs by the Stoner enhancement factor $1/(1-\bar{I})$. According to Altounian and Ström-Olsen [51], the mass enhancement factor is about 2.1–2.2 and the Stoner enhancement factor is 5–8 for amorphous $Ni_xZr_{1-x}$, $0.20 \leqslant x \leqslant 0.67$. The uncertainty in the determination of the enhancement factors should be kept in mind when we compare the calculated DOS with the experimental estimates (figure 5). For the glassy alloys, theory shows that on alloying with Ni, the DOS at $E_F$ decreases up to $x \simeq 0.65$, in agreement with experiment. In the Ni-rich range, an increase in the DOS is predicted. Amorphous $Ni_{85}Zr_{15}$ and crystalline $Ni_5Zr$ show a strong slope in the DOS at $E_F$, which falls short of the critical value for magnetic ordering, in agreement with the observation of Amamou *et al* [46].

### *4.2. Co–Zr alloys*

*4.2.1. Crystalline Co–Zr compounds.* The crystallographic data for the Co–Zr compounds covered in this study are summarized in table 3. The electronic DOS shows essentially the same pattern as in the Ni–Zr compounds: the low-lying part of the band is dominated by the Co states, around the Fermi energy Co and Zr states are strongly hybridized and the upper part of the band is dominated by Zr states (figure 6). In the trigonal prismatic $BRe_3$-type compound $CoZr_3$, there are two inequivalent Zr sites, but with almost no difference in the local DOS. The occurence of trigonal prismatic compounds of $BRe_3$, $Fe_3C$, CrB, FeB types is characteristic for many glass-forming systems, not only for inter-transition metal, but also for transition-metal–metalloid and simple-metal glasses. The electronic structure of $CoZr_3$ differs significantly from that of the isostructural compound $ZnCa_3$ [52]. We take this as an indication that the formation of the $BRe_3$ structure (trigonal $Re_6B$ prisms, arranged in base-sharing columns) depends not so much on the directional properties of the bonds (d–d bonds in $CoZr_3$, p–p bonds in $ZnCa_3$), but on a large size-ratio and strong unlike-atom bonds arising from a strong hybridization of the valence states. The $CuAl_2$-type compound $CoZr_2$ is very similar, only with a slightly broader Co band and a more pronounced hybridization-induced minimum in the DOS just above the Fermi level. The DOS is very similar to that of the isostructural compound $NiZr_2$, except for a slight shift of the Fermi level arising from the reduced number of d electrons.

The effect of a preferred heterocoordination is very strong in the CsCl-type CoZr compound. In the CsCl structure there are no direct like-atom nearest neighbours.

**Table 3.** Crystallographic data of Co–Zr intermetallic compounds, Wigner–Seitz radii, number of $k$-points for Brillouin-zone integration.

| Phase | Pearson symbol | Lattice constant ($nm$) | $R_{Zr}/R_{Co}$ | Number of $k$-points |
|---|---|---|---|---|
| $CoZr_3$ | oC16 | $a = 0.327$<br>$b = 1.084$<br>$c = 0.894$ | 1.26 | 140 |
| $CoZr_2$ | tI12 | $a = 0.6364$<br>$c = 0.5518$ | 1.26 | 90 |
| CoZr | cP2 | $a = 0.3197$ | 1.24 | 165 |
| $Co_2Zr$ | cF24 | $a = 0.69512$ | 1.225–1.35 | 89 |

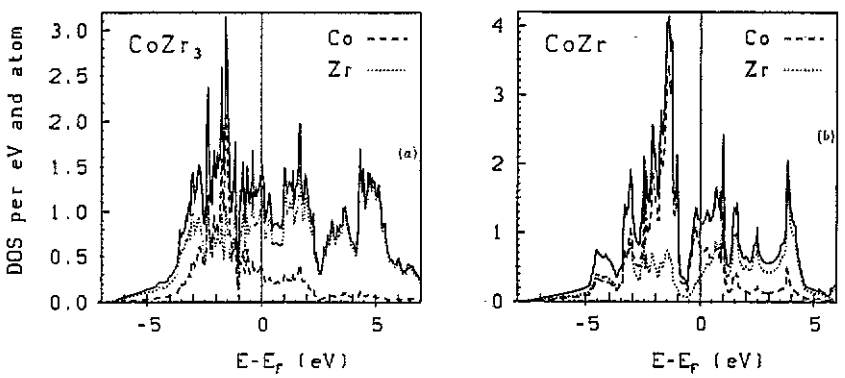


**Figure 6.** Total and site-decomposed electronic density of states in the crystalline compounds $CoZr_3$ ($BRe_3$ type) (*a*) and CoZr (CsCl type) (*b*). Full curve, total DOS; broken curve, Co DOS; dotted curve, Zr DOS.

This leads to a very pronounced minimum in the DOS about 0.7 eV below $E_F$, induced by the narrowing of the Co and Zr bands in the absence of direct Co–Co and Zr–Zr neighbours. Note, however, that the overall form of the DOS is very similar in CrB-type NiZr and CsCl-type CoZr. It must be left to a more detailed future study to elucidate the reasons for the difference in structural stability.

$CoZr_3$, $CoZr_2$ and CoZr are found to be stable in the paramagnetic state, in accordance with the Stoner criterion. The Laves-phase $Co_2Zr$ is a marginal case. A non-spin-polarized calculation predicts a Co DOS of $n_{Co}(E_F) = 1.96$ states $eV^{-1}$ $atom^{-1}$, falling just short of the limiting value of the Stoner theory. Spin-polarized calculations predict a spin-splitting of 0.15 eV accompanied by a small deformation of the spin-split bands (figure 7). The calculation predicts a Co moment of $\mu_{Co} = 0.16\mu_B$ and a negative moment $\mu_{Zr} = -0.05\mu_B$ for Zr, so that $Co_2Zr$ should be weakly ferrimagnetic. The negative Zr moments arise from the strong covalent coupling of the Zr and Co states. Because the Co spin-up states are shifted to lower energies, this coupling is more pronounced in the spin-down bands. Such a 'covalent magnetism' is characteristic for all magnetic alloys of Fe, Co and Ni with 'early' transition metals [3,57]. Experimental investigations of stoichiometric $Co_2Zr$ find no indication for magnetic ordering down to $T = 4.2$ K [53,54]. However, non-stoichiometric $Co_xZr$ becomes ferromagnetically ordered for compositions $2.8 < x <$

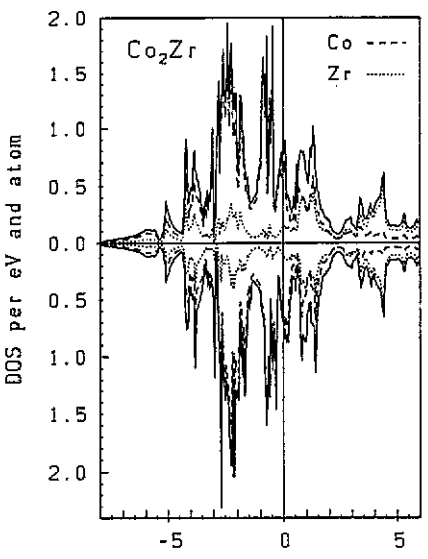


**Figure 7.** Spin-polarized density of states for the Laves phase $Co_2Zr$ ($Cu_2Mg$ type). For key, see figure 6.

3.0, without changing the crystal structure [54]. Ferromagnetism is also induced by partial substitution of Co with Fe, in $(Fe_{1-x}Co_x)_2Zr$ weak ferromagnetism is observed for $x = 0.3$–$0.4$ and mictomagnetism for $x = 0.5$–$0.7$ [55,56].

The magnetic properties also depend quite sensitively on the density. A reduction of the lattice constant by 1% reduces the moments from $\mu_{Co} = 0.16\mu_B$ to $\mu_{Co} = 0.04\mu_B$ and from $\mu_{Zr} = -0.04\mu_B$ to $\mu_{Zr} = -0.01\mu_B$. If the lattice constant is reduced by 1.5%, $Co_2Zr$ becomes paramagnetic. The conclusion to be drawn is that $Co_2Zr$ is just at the boundary between paramagnetism and ferrimagnetism. This is in agreement with the electronic specific heat and susceptibility data, which demonstrate that there is a very large Stoner enhancement [56].

In a case where one is so close to the onset of magnetic ordering, it is important to check the sensitivity of the results to the parameters of the model, i.e. to the choice of the Wigner–Seitz radii and of the exchange-correlation functional. At the radius ratio $R_{Zr}/R_{Co} = 1.225$ corresponding to the ideal packing conditions in a Laves phase and minimal overlap of the atomic spheres, we obtain a nominal charge transfer of 0.062 electrons per Co atom from Zr to Co because of the overlap of the extended Zr states into the Co spheres. An increase of the radius ratio reduces the charge transfer. Neutral atomic spheres are obtained for $R_{Zr}/R_{Co} = 1.26$, but the magnetic moments are still $\mu_{Co} = 0.13\mu_B$ and $\mu_{Zr} = -0.04\mu_B$. The paramagnetic solution is stable only at $R_{Zr}/R_{Co} = 1.35$. Replacing the von Barth–Hedin exchange-correlation functional [44] with Janak's parametrization [64] the Vosko–Wilk–Nusair [58] functional leads to a slight reduction of the Co moments by 0.02 $\mu_B$ and of the Zr moments by $0.01\mu_B$.

Our reference to Stoner theory deserves a brief comment. In a single-component system the Stoner criterion is $In(E_F) \geqslant 1$ where $I$ is an interaction parameter (the Stoner parameter) and $n(E_F)$ is the paramagnetic density of states (per spin) at the Fermi level. According to experimental evidence [41], the Stoner parameter is a constant $I \approx 1$ eV$\mu_B^{-1}$ for magnetic transition-metal systems. In an alloys, one has to use a generalized Stoner-criterion. However, for the (Fe, Co, Ni)–Zr alloys we find

that the magnetic moment on the Zr sites is induced by covalent interactions. This means that the formation of a magnetically ordered state depends primarily on the interactions in the (Fe, Co, Ni) band. For this reason, the simple form of the Stoner criterion is still a useful guide for these alloys.

*4.2.2. Amorphous Co–Zr alloys.* Figure 8 shows the spin-polarized DOS of amorphous $Co_xZr_{1-x}$ alloys with $x = 0.33, 0.50, 0.67, 0.75$ and $0.90$. $a$-$Co_{33}Zr_{67}$ is stable in the paramagnetic state; the calculated DOS is very similar to that of crystalline $CoZr_2$: a narrow Co band with a peak at $-1.7$ eV below $E_F$, a rather flat DOS from $-1$ eV to $+6$ eV, with a minimum at $\simeq 2$ eV and a Zr-dominated peak at $\simeq 5$ eV above $E_F$.

The electronic DOS of $a$-$Co_{50}Zr_{50}$ differs from that of crystalline CoZr only by the absence of the DOS minimum just below $E_F$. The DOS minimum is still present in the Zr DOS, but in the Co DOS it is covered up by the disorder-induced broadening of the Co band. Amorphous $Co_{50}Zr_{50}$ is very close to the onset of magnetism. In our supercell calculations this is reflected by the appearence of isolated magnetic moments on Co sites. In a 64-atom cell we find one Co atom with a magnetic moment of $\simeq 0.5\mu_B$.

Amorphous $Co_{67}Zr_{33}$ and $Co_{75}Zr_{25}$ are both predicted to be ferrimagnetic. The Co bands reflect the strong bonding–antibonding splitting that is also characteristic for the Laves phase $Co_2Zr$. The disorder-induced broadening leads to an increase of the DOS at $E_F$. As a consequence, the onset of magnetism occurs at lower Co content than in the crystalline intermetallic compounds. The formation of the magnetic moments does not lead to a rigid splitting of the majority and minority bands. The Co spin-up band is always narrower than the Co spin-down band. Due to the broadening of the Co spin-down band, the minimum in the Zr DOS is shifted from just below $E_F$ for spin-up electrons to just above $E_F$ for spin-down electrons. Thus the spin-down DOS dominates the occupied Zr band.

For the amorphous alloy, the Fermi level falls into the low-intensity tail of the Co-majority band, where the s and p contribution to the Co DOS is largest. Hence the Co–Zr glasses show strong ferromagnetism. This agrees with the investigation of Shirakawa *et al* [59], who showed that there is no thermal expansion anomaly in $a$-$Co_xZr_{1-x}$. That again suggests strong magnetism.

The variation of the distribution of the magnetic moments with composition is shown in figure 9. At $x = 0.50$ isolated local moments appear. They are induced by strong local Co–Co interactions. At $x = 0.67$ (corresponding to the composition of the Laves phase), the fluctuations in the magnetic moments are still quite large. This is due to fluctuations in partial local coordination numbers: the formation of a large Co moment requires a high number of Co–Co neighbours. With increasing Co content, the distribution of the Co moments narrows, approaching the distribution predicted for hypothetical pure Co [39].

Only the average moments $\bar{\mu} = x\mu_{Co} + (1-x)\mu_{Zr}$ can be compared with experiment. Figure 10 shows the variation of $\bar{\mu}$ with composition, as predicted by our LSD calculations and compared with the experimental data compiled by Malozemoff *et al* [8]. Magnetism in transition metals is often discussed in terms of the Friedel model [60], i.e.

$$\bar{\mu} = \mu_0 - (1-x)(10 - \Delta z) \tag{3}$$

where $\mu_0$ is the moment of the host and $\Delta z$ is the host-solute valence difference. The underlying assumption is that the solute potential displaces precisely five majority

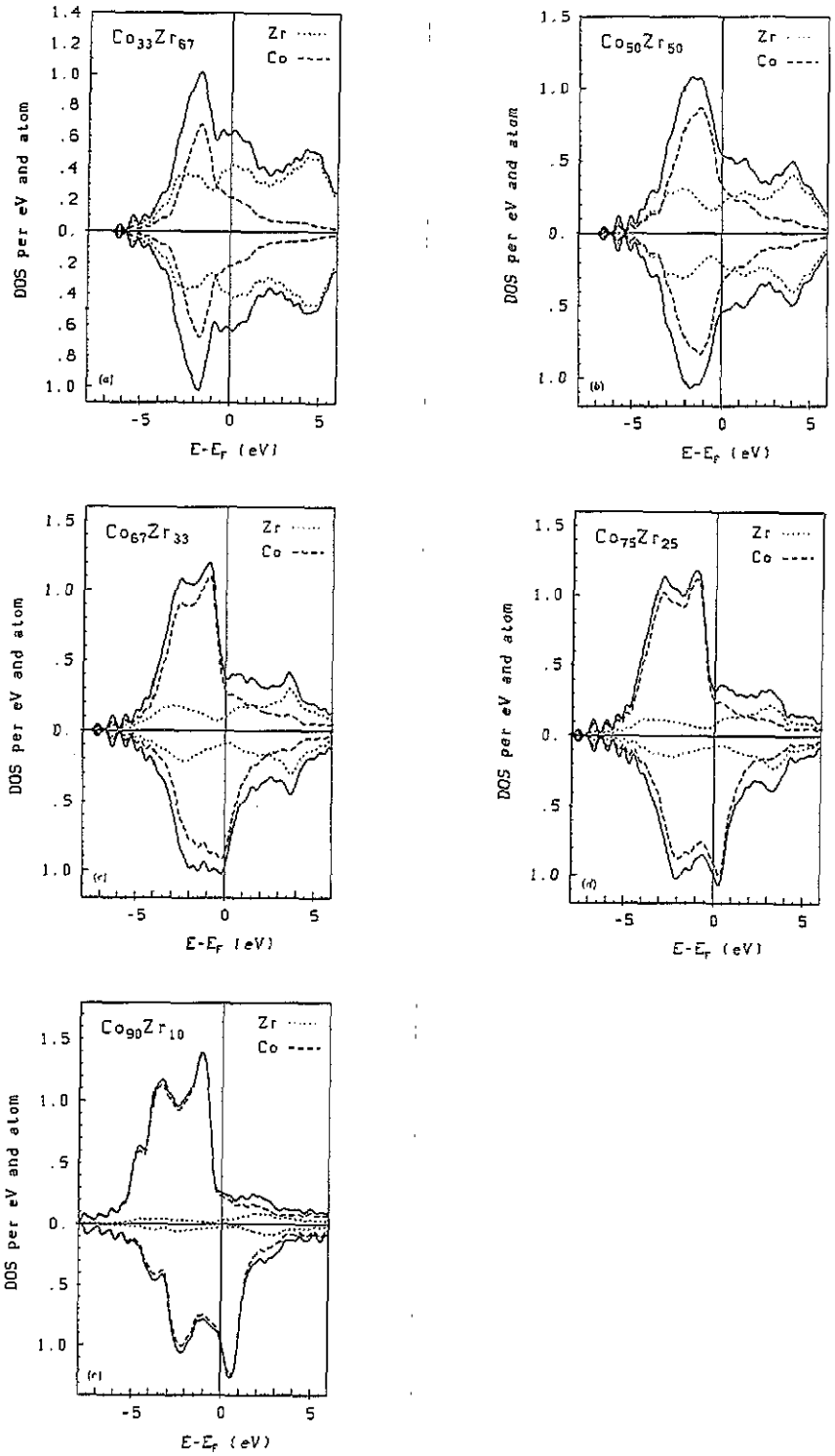


**Figure 8.** Spin-polarized density of states for amorphous $Co_xZr_{1-x}$ alloys with $x = 0.33$, 0.50, 0.67, 0.75 and 0.90 (*a*)–(*e*). For key, see figure 6.

electrons from below to above the Fermi level. For amorphous Co, we calculate a magnetic moment of $\mu_0 = 1.64\mu_B$, which is nearly the same as that calculated for HCP Co ($\mu_0 = 1.55\mu_B$ [61], $\mu_0 = 1.60\mu_B$ [62]) and for FCC Co ($\mu_0 = 1.58\mu_B$ [61], $\mu_0 = 1.56\mu_B$ [62,63]) and in good agreement with the experimental value of $\mu_0 = 1.55\mu_B$, $\mu_0 = 1.7\mu_B$ [6,7]. With this value of $\mu_0$, it is expected that magnetic ordering in $Co_xZr_{1-x}$ disappears at $x = 0.67$, i.e. very close to the composition of the Laves phase (cf above), but at substantially lower solute concentrations than predicted by the LSD calculations for $a$-Co–Zr (see figure 10). The important point is not so much a detailed agreement with this simple rule, but that the Friedel model serves as a reference value: moments lying lower than indicated by the formula would suggest a violation of the basic assumption of strong magnetism, the higher moments found in the LSD calculation and in the experiment confirm the strong magnetism of Co–Zr alloys. However, the physical mechanism for the reduction of the average moment is more complex than the simple Friedel picture: initially, the Co moment decreases much more slowly than corresponding to the linear variation of equation (3), but the strong covalent coupling induces a negative Zr moment, so that the average moment follows approximately equation (3).

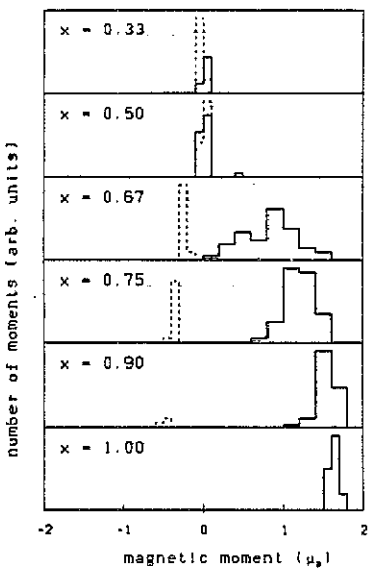


**Figure 9.** Distribution of the magnetic moments in amorphous $Co_xZr_{1-x}$ alloys and in pure amorphous Co. Full curves, Co moments; broken curves, Zr moments.

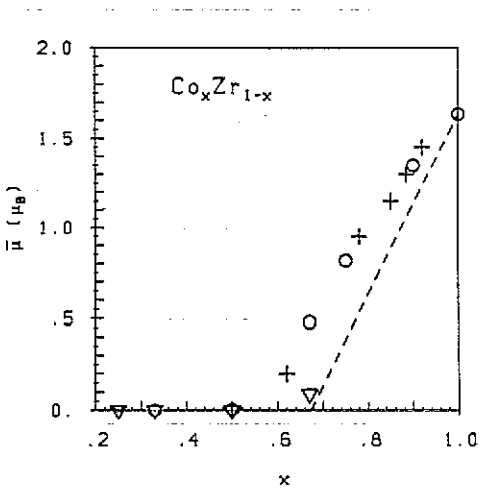


**Figure 10.** Variation of the average magnetic moment in Co–Zr alloys: circles, $a$-Co–Zr, LSD calculation; crosses, $a$-Co–Zr, experimental data as compiled by Malozemoff *et al* [8]; triangles, LSD calculation for crystalline Co–Zr compounds. Straight line, prediction of the Friedel model, see text.

### *4.3. Fe–Zr alloys*

*4.3.1. Crystalline Fe–Zr compounds.* The crystallographic data for the Fe–Zr compounds are summarized in table 4. Figure 11 shows the non-spin-polarized DOS

for $FeZr_3$ ($BRe_3$ type). The electronic structure of $FeZr_3$ is very similar to that of the isostructural compound $CoZr_3$ (figure 6). The DOS at the Fermi level is slightly higher in the Fe compound, but still below the critical value for magnetic ordering. In paramagnetic $FeZr_2$ and $Fe_2Zr$ we find $n_{Fe}(E_F) = 2.27$ states $eV^{-1}atom^{-1}$ and $n_{Fe}(E_F) = 2.28$ states $eV^{-1}atom^{-1}$, respectively. Hence both compounds should be magnetic (we refer to our comments on the Stoner criterion in subsection 4.2). The LSD calculations show that both compounds are ferrimagnetic. In $FeZr_2$ we have $\mu_{Fe} = 0.27\mu_B$ and $\mu_{Zr} = -0.03\ \mu_B$ and in $Fe_2Zr$ $\mu_{Fe} = 1.85\mu_B$ and $\mu_{Zr} = -0.51\mu_B$. Our values for the Laves phase are in very good agreement with the augmented spherical-wave calculations of Mohn and Schwarz [3] ($\mu_{Fe} = 1.90\mu_B$, $\mu_{Zr} = -0.56\mu_B$). The calculated average moment per Fe atom of $\bar{\mu} = 1.60\mu_B$ agrees very well with magnetization measurements yielding $\bar{\mu} = 1.6\mu_B$, resp. $\bar{\mu} = 1.62\mu_B$ [56, 65].

**Table 4.** Crystallographic data of Fe–Zr intermetallic compounds, Wigner–Seitz radii, number of $k$-points for Brillouin-zone integration.

| Phase | Pearson symbol | Lattice constant ($nm$) | $R_{Zr}/R_{Fe}$ | Number of $k$-points |
|---|---|---|---|---|
| $FeZr_3$ | oC16 | $a = 0.3324$<br>$b = 1.099$<br>$c = 0.8810$ | 1.25 | 140 |
| $FeZr_2$ | tI12 | $a = 0.6385$<br>$c = 0.5596$ | 1.24 | 165 |
| $Fe_2Zr$ | cF24 | $a = 0.7074$ | 1.225 | 505 |

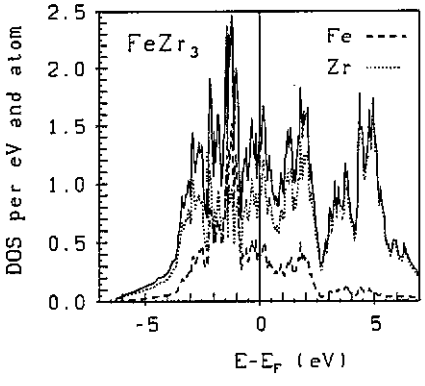


**Figure 11.** Total and site decomposed density of states in the crystalline compound $FeZr_3$ ($BRe_3$ type). Full curve, total DOS; broken curve, Fe DOS; dotted curve, Zr DOS.

In the spin-polarized DOS (figure 12), we find only a small exchange-splitting in $FeZr_2$ ($CuAl_2$ type), but pronounced differences between the DOS of majority and minority electrons in $Fe_2Zr$ ($Cu_2Mg$ type). In the non-spin-polarized DOS the Fermi level falls into a region of high values between 1 eV above and below $E_F$. In the spin-up bands, the upper DOS minimum becomes very broad, in the spin-down bands the lower minimum is more pronounced. The deviations from a rigid-band behaviour are even more pronounced for the Zr states. The upper part of the band, which is only weakly coupled to the Fe states, is nearly unaffected by spin polarization. The

lower part of the band is characterized by a strong coupling between the Zr states and the Fe spin-down states. The ferrimagnetic character is a consequence of this strong covalent coupling, as discussed by Mohn and Schwarz [3]. The Fe–Zr compounds are weak ferrimagnets, at all compositions there is a Fe-d peak in the spin-up DOS above the Fermi level.

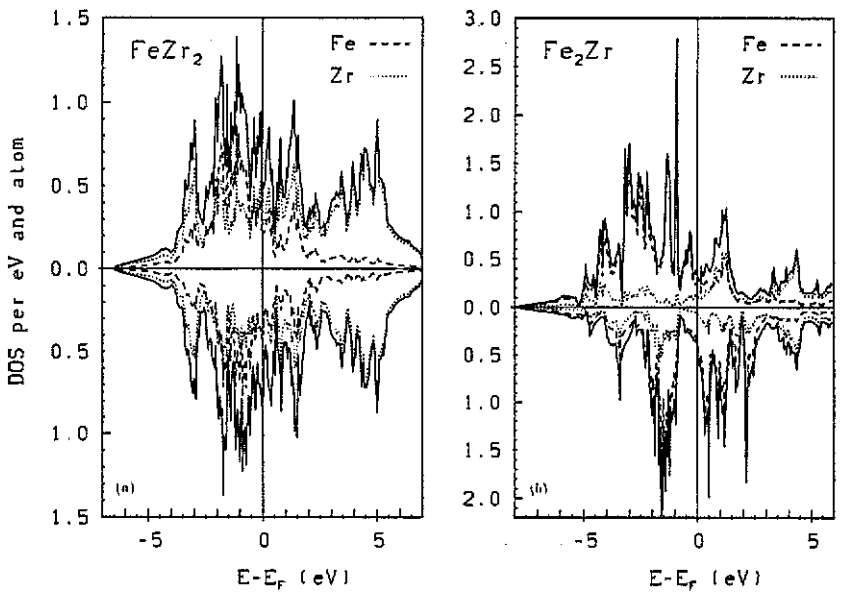


**Figure 12.** Spin-polarized density of states for the compounds $FeZr_2$ ($CuAl_2$ type) (*a*) and $Fe_2Zr$ ($Cu_2Mg$ type) (*b*). For key, see figure 11.

With $\mu_0 = 2.2\mu_B$ for BCC Fe [63], magnetism in $Fe_xZr_{1-x}$ should vanish for $x \leqslant 0.45$ according to the Friedel model, whereas $FeZr_2$ is still weakly ferrimagnetic (figure 12).

*4.3.2. Amorphous Fe–Zr alloys.* Amorphous Fe–Zr alloys belong to the best investigated amorphous magnets. The interest in these materials arises from the complex spin-structures of the Fe-rich glasses. A detailed molecular-dynamics study of Fe–Zr glasses is described in [27]. Spin-polarized electronic structure calculations have been performed for $Fe_xZr_{1-x}$ glasses with $x = 0.24, 0.33, 0.50, 0.67, 0.75, 0.90$ and 0.95. The spin-polarized densities of states are shown in figure 13. The onset of magnetic ordering occurs at $x \simeq 0.33$, where we find localized, strongly fluctuating Fe moments but an average moment that is still slightly lower than in crystalline $FeZr_2$. The reason is that in crystalline $FeZr_2$ the Fermi energy falls onto a peak in the DOS which is smeared out by the structural disorder. For higher Fe concentrations (but $x \leqslant 0.80$) the averaged magnetic moments in the amorphous alloys are exactly equal to those in the corresponding crystalline compound. Indeed the electronic DOS of $a$-$Fe_{67}Zr_{33}$ is just a smeared-out version of that of the Laves-phase $Fe_2Zr$. This corroborates the conclusion drawn on the basis of our structural modelling studies that the local order in the glassy phase is very similar to that in the crystalline phase.

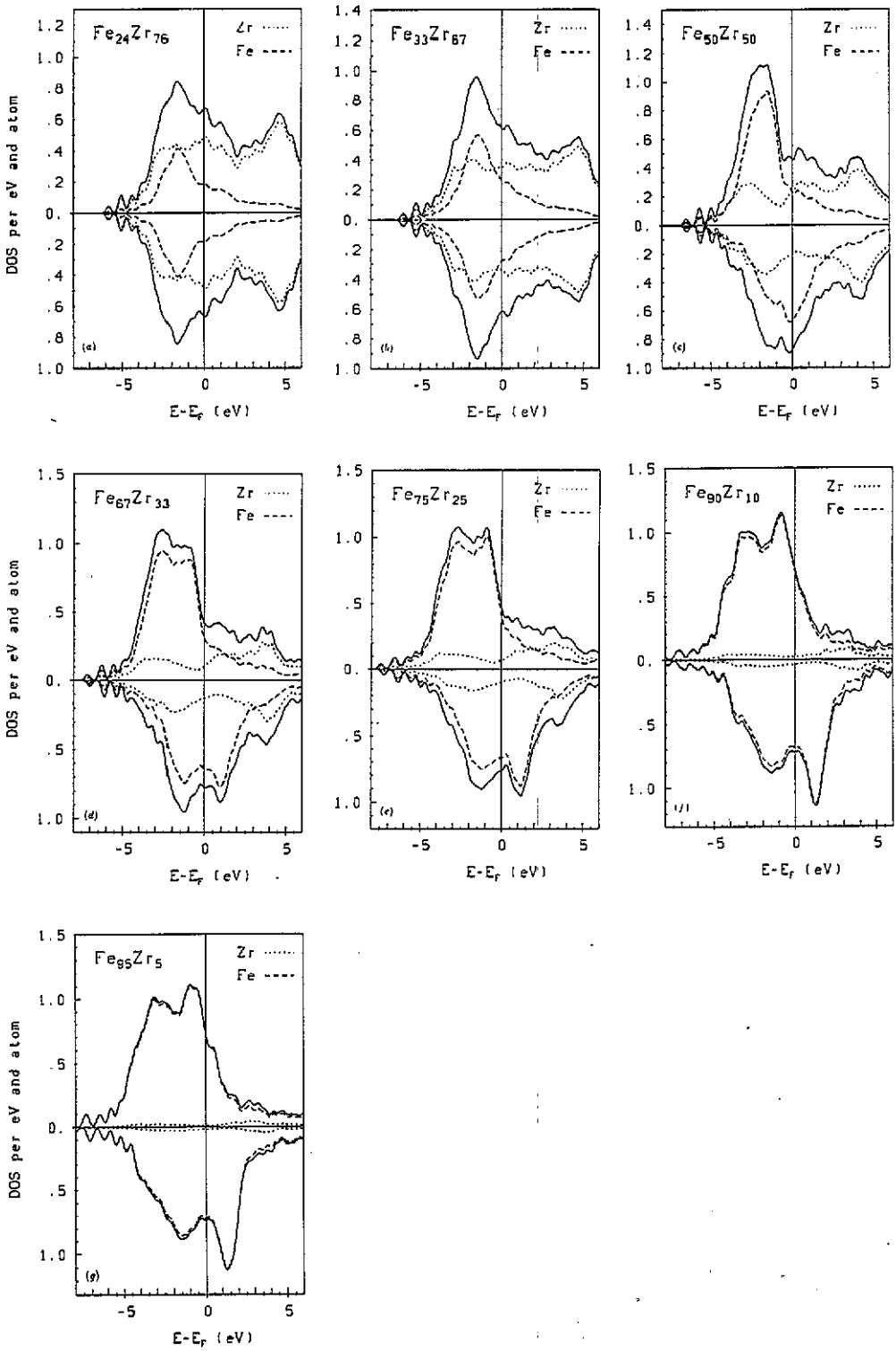


**Figure 13.** Spin-polarized density of states for amorphous $Fe_xZr_{1-x}$ alloys with $0.24 \leqslant x \leqslant 0.95$ $(a)$–$(g)$. For key, see figure 11.

An interesting result appears at larger Fe content: at $x = 0.75$, one isolated Fe atom has a large negative moment ($\mu \simeq -1.3\mu_B$). At even larger Fe concentrations the magnetization of the Fe atoms acquires an antiferromagnetic component. This happens not by a broadening of the distribution of the ferromagnetic moments into the negative region; rather we find two relatively narrow distributions centred at large positive and negative values. We have taken particular care to establish that the occurence of negative moments is not a computational artefact. For $x = 0.90$ and $x = 0.95$ the supercell calculations were repeated for several independent atomic configurations of the supercell. Negative Fe moments were found in all configurations.

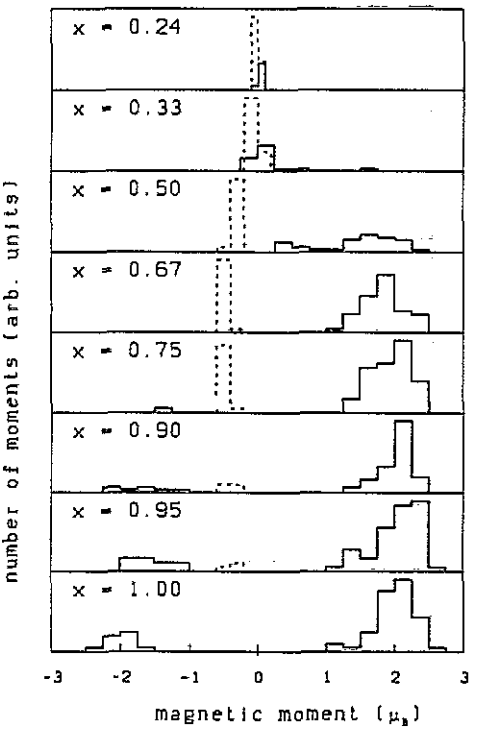


**Figure 14.** Distributions of the magnetic moments in amorphous $Fe_xZr_{1-x}$ alloys and in amorphous Fe as a function of composition. Full curves, Fe moments; broken curves, Zr moments.

The evolution of the distribution of magnetic moments as a function of composition is shown in figure 14. We also include our results for pure amorphous Fe at a density of $\rho = 7.92$ g cm$^{-3}$, corresponding roughly to the density of BCC iron. The present results for the $a$-Fe–Zr alloys extrapolate quite well to the result for the pure metal. However, the results for dilute Zr concentrations depend on the particular configuration. This reflects the strong local-environment effect. It also corresponds to the scattering of the experimental data caused by slight differences in the preparation conditions. It is desirable to test the predicted distributions against experimental data, e.g. hyperfine field distributions from Mössbauer spectroscopy. Unfortunately, the published data [12, 13, 67, 68] are somewhat controversial. The conversion of the most recent hyperfine data [12, 13] to a magnetic moment distribution according to $B_{hf} = A|\mu_{Fe}|$ with $A = 13$ T$\mu_B^{-1}$ yields reasonable agreement between theory and experiment. In particular the experiment seems to confirm the predicted absence

of a paramagnetic component in the distribution of the Fe moments (figure 15). However, in view of the well known difficulties in extracting reliable hyperfine field data from Mössbauer spectra [69] and since the $B_{hf}$–$\mu_{Fe}$ proportionality has been well established only for the core contribution to $B_{hf}$ (which is the dominating part of the total $B_{hf}$) [70], this point deserves further investigation.

The predicted average moments are in very good agreement with the experimental data (figure 16) throughout the entire composition range, for the crystalline as well as the amorphous phases.

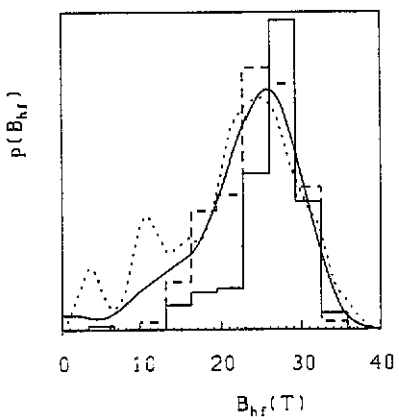


**Figure 15.** The calculated distribution of the Fe moments $|\mu_{Fe}|$ in $Fe_xZr_{1-x}$ alloys with $x = 0.90$ (full histogram) and $x = 0.95$ (broken histogram) against the experimental distribution of the hyperfine fields $B_{hf}$ for $x = 0.90$ (full curve, [13]) and $x = 0.93$ (dotted curve, [12]).

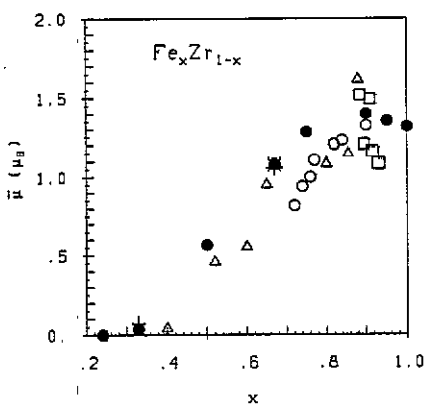


**Figure 16.** Average magnetic moments $\bar{\mu}$ in crystalline and amorphous Fe–Zr alloys. Full dots, *a*-Fe–Zr, theory; open symbols, *a*-Fe–Zr, experiment (circles, as compiled in [8]; squares, [12]; triangles, [66]); +, *c*-Fe–Zr, theory; ×, *c*-Fe–Zr, experiment ([56,65]).

At present, photoemission results are available only for the Zr-rich paramagnetic alloys. Experimental as well as theoretical investigations of the photoelectron spectra of the magnetic amorphous $Fe_xZr_{1-x}$ alloys are under way and will be reported in due course.

The prediction of positive and negative Fe moments in the Fe-rich alloys correlates well with the observed non-collinear spin structures. Note that in our calculations the magnetic moments are constrained to only two possible directions: up and down. Recently several attempts have been made to relax this restriction, both in the local spin-density [71,72] and in the tight-binding [73] framework. It is not yet clear whether the self-consistent LSD calculations for non-collinear spins will be feasible for amorphous supercells. In the TB calculations, a large initializing field is necessary to start the calculation. Even though the field is reduced to zero in the iteration process, the final result depends quite sensitively on the geometry of the initializing field [73]. For the moment, the prediction of competing ferromagnetic and antiferromagnetic exchange interactions by *ab initio* calculations is certainly a remarkable result.

## 5. Competing ferromagnetic and antiferromagnetic exchange interactions in $\alpha$-Fe and $\alpha$-$Fe_xZr_{1-x}$

### *5.1. Local environment effect*

The question is now for the origin of the antiferromagnetic Fe moments. The first point to note is that there is no correlation between the negative Zr moments and the negative Fe moments. This is demonstrated in figure 17 which shows an instantaneous configuration of $Fe_{90}Zr_{10}$, projected onto a plane: there are no local correlations between the Zr sites and negative Fe moments. The different character of the negative Fe and Zr moments is also evident from the spin-densities: figure 18 shows the radial spin-densities $\Sigma(r) = 4\pi r^2\sigma(r)$, $\sigma(r) = \rho^{\uparrow}(r) - \rho^{\downarrow}(r)$, inside the atomic spheres of $\alpha$-$Fe_{90}Zr_{10}$. For the Fe sites, the average has beeen taken over sites with positive and negative moments separately. We notice that on the Fe sites, the spin density is localized well inside that atomic sphere, independent of the direction of the moment. Around Zr, the spin density is small in the core region, but increases steadily towards the boundary of the atomic sphere. A similar result had been found by Mohn and Schwarz for the Laves phase $Fe_2Zr$ [3]. It demonstrates again that the negative spin-density of Zr is induced by interaction with the neighbouring Fe atoms.

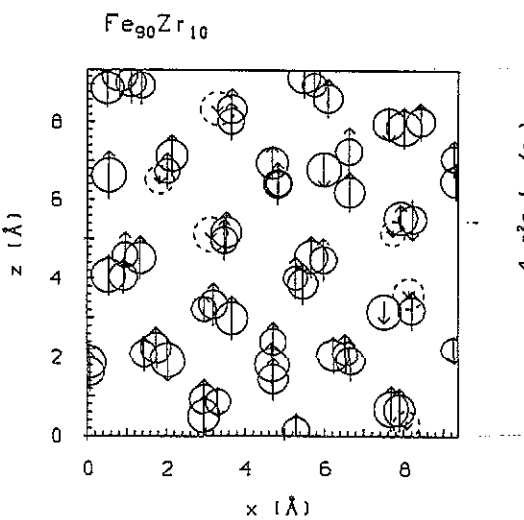


**Figure 17.** Projection of a 64-atom model for amorphous $Fe_{90}Zr_{10}$ onto the $(x, z)$ plane. The size of the circles representing the atoms (full curves, Fe; broken curves, Zr) is scaled with the $y$ coordinate, the arrows indicate the magnitude and direction of the local magnetic moment.

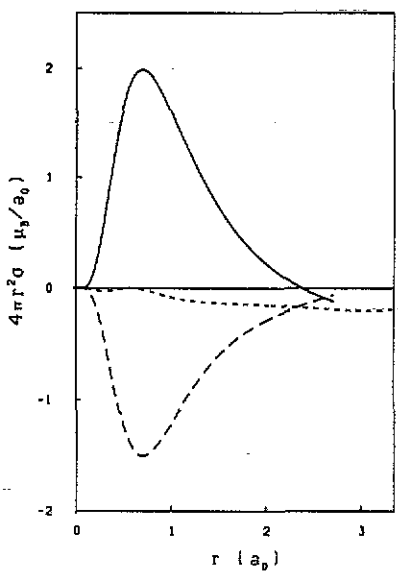


**Figure 18.** Radial spin densities $\Sigma(r) = 4\pi r^2\sigma(r)$ inside the atomic spheres of amorphous $Fe_{90}Zr_{10}$. Full curve, averaged over Fe-sites with positive moments; long-dash curves, averaged over Fe sites with negative moments; short-dash curve, averaged over Zr sites.

The next step is to look for correlations between the local moments and local structural information such as the local atomic volume or the coordination number. A detailed study of such correlations has already been presented for amorphous Fe [39]. The essentially negative result has been confirmed here for $\alpha$-$Fe_xZr_{1-x}$:

although there is a general correlation between a large local volume and a large moment, this holds for positive and negative moments alike. There are also no correlations between the local moment and the local Fe–Fe coordination number $N_{FeFe}$ ($N_{FeFe}$ being defined as the number of Fe neighbours at distances up to the distance corresponding to the first minimum of the partial pair distribution function). Hence the formation of negative moments depends in a more subtle way on the local environment.

Local environment effects in amorphous transition metals have been discussed in a more phenomenological way by Kakehashi [75] using a functional-integral approach to the degenerate-band Hubbard model. Kakehashi predicts that the local magnetic moment on an atom depends on the number of contracted atoms in its nearest-neighbour shell (i.e. of atoms with short distances to the central site). The central moment is positive, negative or negligible if the number of contracted atoms is small, medium or high, respectively.

Evidently, this is correlated to the transition from ferromagnetism at low density to antiferromagnetism at high density in close-packed crystalline Fe. According to recent LSD calculations, this transition occurs in FCC Fe at a nearest-neighbour distance of $d_{NN} = 2.575$ Å [76] or $d_{NN} = 2.594$ Å [77], and in HCP Fe at $d_{NN} = 2.633$ Å [78]. The detailed analysis of our LSD results confirms Kakehashi's ideas. In the magnetically ordered $Fe_xZr_{1-x}$ alloys ($x \geqslant 0.33$), the first peak in the Fe–Fe correlation function occurs at distances between $d_1 = 2.59$ Å (at $x = 0.33$) and $d_1 = 2.49$ Å (at $x = 0.90$ Å). However, the width of the peak shows that nearest-neighbour distances scatter from 2.2 Å to 3.4 Å (see [27]). We find that—as proposed by Kakehashi—there is a correlation between a negative moment on the central Fe atom and a high number of contracted nearest Fe neighbours, i.e. neighbours with distances up to or only slightly larger than the position of the peak in the pair correlation function (i.e. at distances smaller than 2.6 to 2.8 Å, depending on composition). The degree of this correlation is presented in figure 19 for $a$-Fe, $a$-$Fe_{90}Zr_{10}$ and $a$-$Fe_{75}Zr_{25}$. The particular value of our cutoff distance (2.6–2.8 Å) is close to the nearest-neighbour distance for the transition between ferromagnetic and antiferromagnetic state in crystalline FCC and HCP iron.

Thus our results show that there is not only a global change of sign in the exchange interaction with increasing density, but also a change of sign in the local exchange coupling between two atoms once the pair-distance shrinks below a critical value. Locally, a strong tendency to spin-flip occurs once the number of contracted pairs (and negative exchange interactions) outweighs those at larger distances (and positive exchange interactions). The actual calculation of exchange interactions in disordered spin configurations from the LSD result remains a challenge. The highly local character of the magnetic interaction is also evident from the variation of the local DOS with the local moment.

### *5.2. Correlation between local moments and local density of states*

There are also strong correlations between the local magnetic moments and the local density of states and hence between fluctuations in the moments and fluctuations in the self-consistent potentials. Figure 20 shows the site and angular momentum decomposed local densities of states for $a$-$Fe_{90}Zr_{10}$, averaged over Fe sites with positive and negative moments separately and over Zr sites. We find that the local Fe DOS is characteristically different on sites with positive and negative moments: on

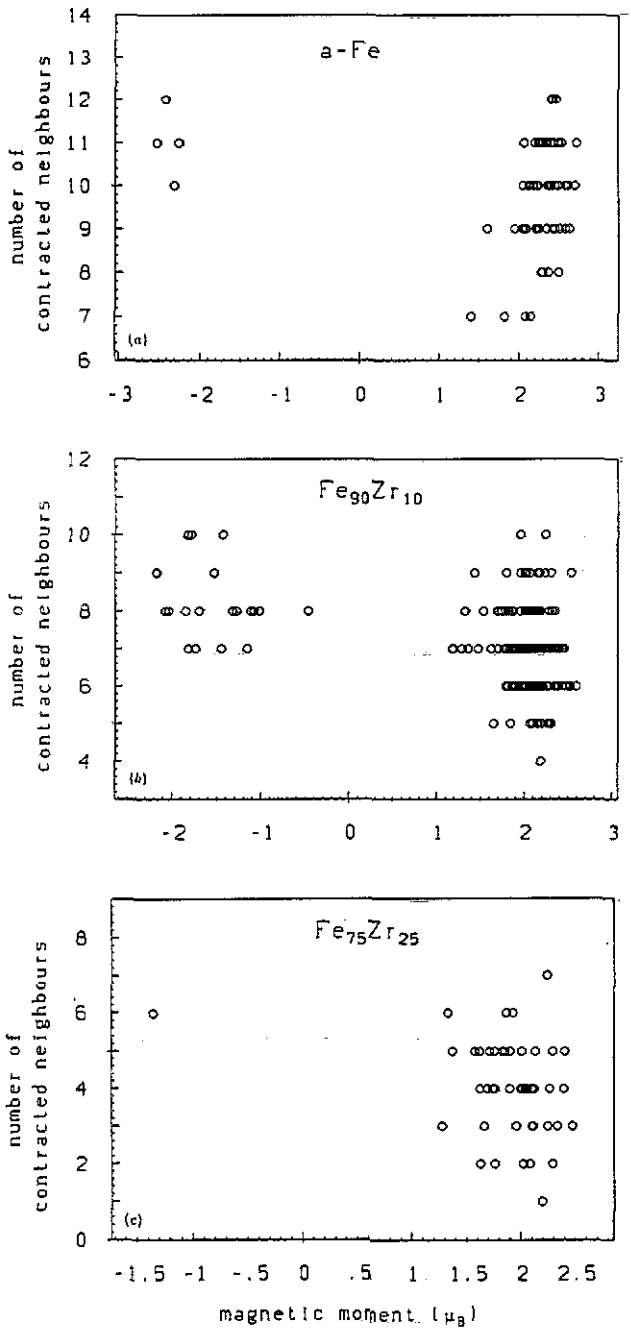


**Figure 19.** Number of contracted Fe neighbours against local magnetic Fe moment in amorphous Fe (*a*), $Fe_{90}Zr_{10}$ (*b*) and $Fe_{75}Zr_{25}$ (*c*). Contracted neighbours are atoms situated at distances smaller than 2.8 Å (*a*), 2.7 Å (*b*) and 2.6 Å (*c*), respectively. These distances are just beyond the position of the first peak in the Fe–Fe correlation function.

the sites with positive moments, the spin-up band is nearly full, in the spin-down band the Fermi level falls into the bonding–antibonding pseudogap. On the sites with negative Fe moment, the spin-up DOS shows a pronounced maximum just above the Fermi level, the maximum in the spin-down DOS is shifted towards the bottom of the band. This suggests that the origin of the antiferromagnetic Fe moments in *a*-Fe–Zr and *a*-Fe (and the absence of such moments in *a*-Co–Zr and *a*-Co) is associated with

the transition from strong to weak magnetism. In a strong magnetic material such as Co and its Zr alloys, the ferromagnetic exchange splitting leads to a completely full spin-up band with a low DOS at $E_F$. This is an energetically favourable stable situation. In a weak magnetic material, the exchange splitting is not sufficient to push the spin-up band completely below $E_F$; the DOS at $E_F$ is still quite large. In this situation, a lowering of the electronic ground-state energy is possible by reversing the magnetic polarization on a few Fe sites. The spin-flips create a narrow spin-up band just above $E_F$ and contribute to a reduction of the overall DOS at the Fermi level (see figure 20).

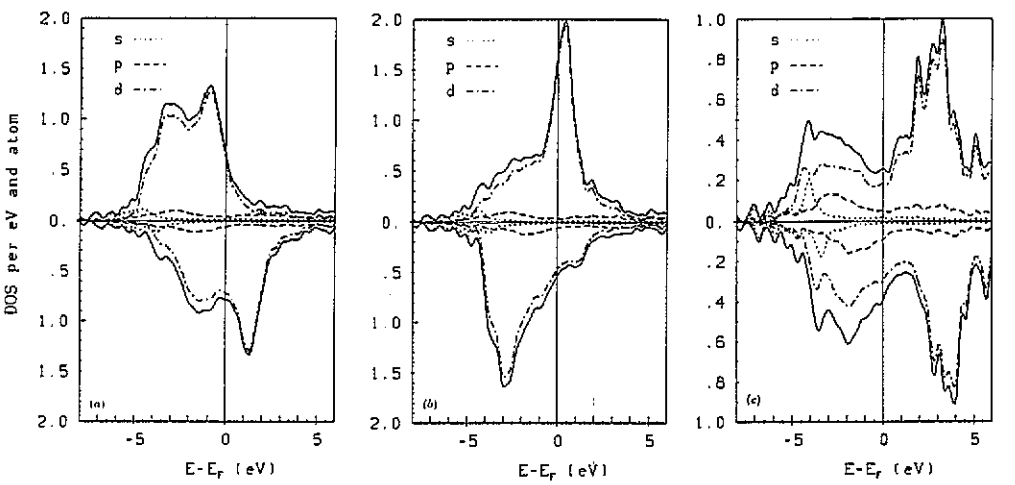


**Figure 20.** Spin-polarized local density of states for amorphous $Fe_{90}Zr_{10}$: (*a*) averaged over Fe sites with positive moments; (*b*) averaged over Fe sites with negative moments; (c) averaged over Zr sites. Full curve, total local DOS; chain curve, d-electron contribution; broken curve, p-electron contribution; dotted curve, s-electron contribution.

## 6. Exchange splitting

Evidently, there is a strong correlation between the local magnetic moment and the local exchange splitting. This correlation is now analyzed in more detail. The local magnetic moment $\mu_R$ is given by the local spin density, integrated over the atomic sphere. The local exchange splitting $\Delta_R$ is given by the potential parameters $C_{Rnlm\uparrow(\downarrow)}$, see section 3. Figure 21 shows that the correlation is linear to a very good approximation. A least-squares fit yields a value of $I = 0.95$ eV$\mu_B^{-1}$ for the ratio $I = \Delta_R/\mu_R$ for the Fe sites. What is even more interesting, we find that this simple proportionality is valid for all crystalline and amorphous Fe–Zr and Co–Zr alloys, independent of composition and for crystalline and amorphous Fe and Co, independent of density (see figure 22). These systems cover a wide range of magnetic states ranging from ferromagnets over antiferromagnets to spin-glass states. This means that the type of magnetic ordering is irrelevant for the exchange splitting, only the local magnetization at a given atomic site counts. A similar result for

the ferromagnetic crystalline 3d metals has been found in earlier LSD calculations [63, 74]. Our results extend this correlation to crystalline compounds and amorphous materials and show that it holds on a local level, irrespective of the existence of a strongly fluctuating magnetization.

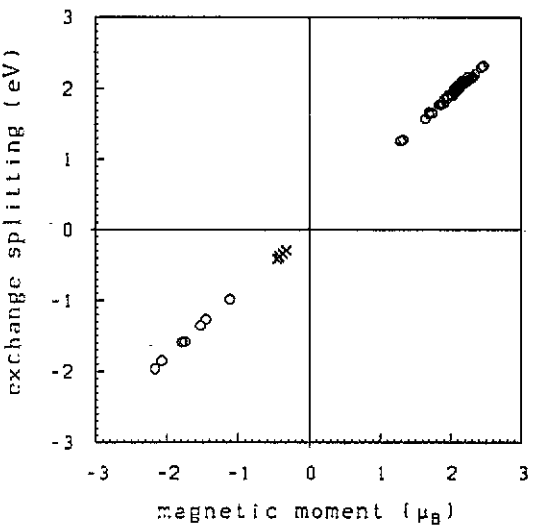


**Figure 21.** Correlation of the local exchange splittings and the local magnetic moments in $a$-$Fe_{90}Zr_{10}$. Circles, Fe; crosses, Zr.

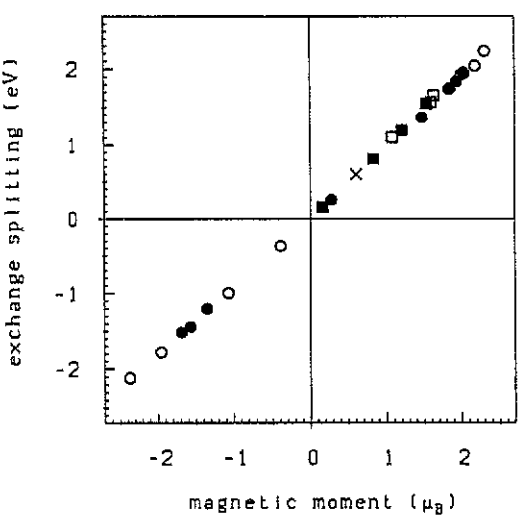


**Figure 22.** Correlation between the average magnetic exchange splitting and the average magnetic moment for crystalline and amorphous Fe, Co and Ni, and for crystalline and amorphous Fe–Zr and Co–Zr alloys. For the Fe systems positive and negative moments are plotted separately. Circles, Fe; squares, Co (open symbols, elements; full symbols, alloys); cross, Ni.

A similar correlation holds for the negative Zr moments (see figure 21). In the Fe-rich $a$-Fe–Zr alloys, the value of $I$ is nearly the same on Zr and Fe sites, whereas at higher Zr content and in $a$-Co–Zr, $I_{Zr}$ is 10–15% lower than $I_{Fe(Co)}$.

From an experimental point of view, the apparent universality of the ratio of the exchange splitting to the magnetic moment has recently been demonstrated by Himpsel [41] for a wide variety of systems, ranging from the ferromagnetic elements

over spin glasses to magnetic overlayers and the free atoms. The experimental value of $I \simeq 1$ eV$\mu_B^{-1}$ is almost identical to our result.

In the theory of itinerant magnetism the ratio of the exchange splitting to the magnetic moment is known as the Stoner parameter, which is essential in determining the magnetic properties such as Curie temperature, susceptibility etc. Within a TB Hubbard approach, the Stoner parameter is replaced by $I_{\text{eff}} = (U + 5J)$, where $U$ and $J$ are the intra-atomic Coulomb and exchange integrals [79]. Thus our result, derived from local spin-density theory, seems to lend some support to TB Hubbard models of itinerant magnetism, based on the assumption of site-independent Coulomb and exchange integrals. However, the origin of this universal correlation remains to be worked out.

## 7. Discussion and summary

We have presented the first self-consistent spin-polarized electronic structure calculations for realistic models of amorphous transition-metal alloys. Our results show that reliable predictions of the magnetic moments in amorphous alloys are possible on the basis of first-principles local-density calculations. The microscopic calculations elucidate the physical mechanism for the formation of the magnetic moments and show that the magnetic amorphous alloys of Co and Fe with Zr are ferrimagnetic like the corresponding crystalline compounds. The negative moments on the Zr sites are induced by a spin-dependent strong covalent coupling of the Zr-d band to the Fe-d states.

Our calculations explain the different magnetic properties of Co–Zr and Fe–Zr glasses. Co–Zr alloys are strong magnets at all compositions, the disorder-induced broadening of the Co-d states leads to an increased Co DOS at $E_F$ in the glass compared to the crystalline compound and hence to enhanced magnetism. In Zr-rich Fe–Zr alloys the Fermi level falls onto a peak in the DOS, which is reduced by the disorder-induced broadening of the bands. Therefore, magnetism is slightly reduced on amorphization. In the Fe-rich glasses the local spin-density calculations predict competing ferromagnetic and antiferromagnetic interactions, which are coupled to local fluctuations in the spin-density potentials. These competing interactions lead to a complex spin structure with positive and negative Fe moments. The appearance of local antiferromagnetic moments in glassy Fe–Zr alloys relates to the global tendency to antiferromagnetism in the unstable close-packed crystalline phases of Fe. In both cases the antiferromagnetic coupling is associated with weak ferromagnetism (incompletely filled majority band) arising from a band broadening induced by the increased interatomic overlap. Our result shows that this mechanism operates also on a strictly local basis. In this context it is also important that we find a strict proportionality between the local magnetic moment and the local exchange splitting, the ratio being the same in the alloys and in the pure metals irrespective of the magnetic order.

Our theory also points to distinct differences between the self-consistent LSD approach and calculations based on parametrized tight-binding Hubbard Hamiltonians. It seems that the tight-binding calculations with fixed transfer integrals and fixed Coulomb integrals underestimate the importance of local fluctuations in the self-consistent potentials and hence lead to different predictions for the distributions of the moments, even though the calculated average moments agree reasonably well.

The advantage of the tight-binding approach is that it is easier to allow for non-collinear spin structures, whereas this is still a challenge with self-consistent LSD calculations.

The difference between the LSD and TB results is probably due to the different description of the exchange coupling. In the usual TB Hamiltonian [21, 73], the magnetic interaction part is not only site diagonal, but also orbital diagonal, i.e. the intra-atomic exchange is neglected and the magnetic behaviour is completely due to the intra-atomic correlation. In the LSD, both correlation and exchange effects are included in the local approximation. Hence it is not surprising that the local interactions are more complex in the LSD than in the TB approximation. However, the relation between the two approximations remains to be worked out in detail.

## Acknowledgments

This work has been supported by the Bundesministerium für Wissenschaft und Forschung within the Materials Research Program. The numerical calculations have been performed at the Computing Centre of the Technische Universität Wien (Siemens-Fujitsu VP50-EX).

## References

[1] Williams A R, Moruzzi V L, Gelatt C D and Kübler J 1983 *J. Magn. Magn. Mater.* **31-34** 88
[2] Schwarz K, Mohn P, Blaha P and Kübler J 1984 *J. Phys. F: Met. Phys.* **14** 2659
[3] Mohn P and Schwarz K 1985 *Physica* **130B** 26
[4] Armitage J G M, Dunelow T, Mitchell R H, Riedi P C, Abell J S, Mohn P and Schwarz K 1986 *J. Phys. F: Met. Phys.* **16** L141
[5] Bieber A and Gautier F 1986 *J. Magn. Magn. Mater.* **54-57** 967
[6] Kwan M L and Hoffmann R W 1974 *Japan. J. Appl. Phys. Suppl.* **2** 3065
[7] Whyman P and Aldridge R V 1974 *J. Phys. F: Met. Phys.* **4** L6
[8] Malozemoff A P, Williams A R, Terakura K, Moruzzi V L and Fukamichi K 1983 *J. Magn. Magn. Mater.* **35** 192
[9] Grigson C W B, Dove D B and Stilwell G R 1984 *Nature* **204** 173
[10] Felsch W 1969 *Z. Phys.* **219** 280
[11] Rhyne J J and Fish G E 1985 *J. Appl. Phys.* **57** 3407
[12] Ryan D H, Coey J M D , Batalla E, Altounian Z and Ström-Olsen J 1987 *Phys. Rev.* B **35** 8630
[13] Ryan D H and Hong Ren 1991 *J. Appl. Phys.* **69** 5057
[14] Saito N, Hiroyoshi H, Fukamichi K and Nakagawa Y 1986 *J. Phys. F: Met. Phys.* **16** 911
[15] Ma H, Kunkel H P and Williams G 1991 *J. Phys.: Condens. Matter* **3** 5563
[16] Gaskell P H 1983 *in Glassy Metals II* ed H Beck and H J Güntherodt (Berlin: Springer) p 5
[17] Suzuki K 1990 *J. Non-cryst. Solids* **117+118** 1
[18] Hausleitner Ch and Hafner J 1992 *Phys. Rev.* **B 45** 115, 128
[19] Mathur P 1983 *Z. Phys.* B **53** 255
[20] Xu Y N, He Y and Ching W Y 1991 *J. Appl. Phys.* **69** 5460
[21] Krauss U and Krey U 1991 *J. Magn. Magn. Mater.* **98** L1
[22] Pettifor D G 1989 *Phys. Rev. Lett.* **63** 2480
[23] Pettifor D G and Aoki M 1991 *Phil. Trans. R. Soc.* A **334** 439
[24] Heine V and Weaire D 1970 *Solid State Physics* vol. 24 ed H Ehrenreich, F Seitz and D Turnbull (New York: Academic) p 247
[25] Hafner J 1987 *From Hamiltonians to Phase Diagrams, Solid State Sciences* vol. 70 (Berlin: Springer)
[26] Hausleitner Ch and Hafner J 1990 *Phys. Rev.* B **42** 5863
[27] Hausleitner Ch and Hafner J 1992 *J. Non-cryst. Solids* (in print)
[28] Hausleitner Ch, Tegze M and Hafner J 1992 *J. Phys.: Condens. Matter* (submitted)

[29] Jaswal S S and Hafner J 1988 *Phys. Rev.* B **38** 7311
[30] Andersen O K, Jepsen O and Glötzel D 1985 *Highlights of Condensed Matter Theory* ed F Bassani, F Fumi and M P Tosi (Amsterdam: North Holland) p 59
[31] Skriver H L 1984 *The LMTO Method* (Berlin: Springer)
[32] Jank W and Hafner J 1990 *Phys. Rev.* B **41** 1497; *Phys. Rev.* B **42** 6296
[33] Hafner J and Jank W 1991 *Phys. Rev.* B **42** 11530; *Phys. Rev.* B **45** 2739
[34] Jank W, Hausleitner Ch and Hafner J 1991 *Europhys. Lett.* **16** 473
[35] Hafner J and Jaswal S S 1988 *Phys. Rev.* B **38** 7320
[36] Andersen O K, Jepsen O and Šob M 1987 *Electronic Band Structure and Its Applications (Lecture Notes in Physics* **283***)* ed M Yussouff (Berlin: Springer) p 1
Fujiwara T 1984 *J. Non-cryst. Solids* **61+62** 1039
[37] Heine V, Haydock R and Kelly M 1980 *Solid States Physics* vol. 35 ed H Ehrenreich, F Seitz and D Turnbull (New York: Academic)
[38] Bose S K, Jaswal S S, Andersen O K and Hafner J 1988 *Phys. Rev.* B **37** 9955
[39] Turek I and Hafner J 1992 *Phys. Rev.* B **46** 247
[40] Krompiewski S, Krauss U and Krey U 1989 *Phys. Rev.* B **39** 2819
[41] Himpsel F J 1991 *Phys. Rev. Lett.* **67** 2363
[42] Villars P and Calvert L D 1985 *Pearson's Handbook on Crystallographic Data for Intermetallic Phases* (Metals Park, Ohio: American Society for Metals)
[43] Kohn W and Sham L J 1965 *Phys. Rev.* **140** A1133
[44] von Barth U and Hedin L 1972 *J. Phys. C: Solid State Phys.* **5** 1629
[45] Amamou A 1980 *Solid State Commun.* **37** 7
[46] Amamou A, Kuentzler R, Dossmann Y, Forey P, Glimois J L and Feron J L 1982 *J. Phys. F: Met. Phys.* **12** 2509
[47] Oelhafen P 1987 *in Liquid and Amorphous Metals* ed E Lüscher, G Fritsch and G Jacucci (Dordrecht: Martinus Nijhoff) p 333
[48] Redinger J, Marksteiner P and Weinberger P 1986 *Z. Phys.* B **63** 321
[49] Jarlborg T and Nilsson P O 1979 *J. Phys. C: Solid State Phys.* **12** 265
[50] Jank W and Hafner J 1990 *J. Phys.: Condens. Matter* **2** 5065
[51] Altounian Z and Ström–Olsen J O 1983 *Phys. Rev.* B **27** 4149
[52] Tegze M and Hafner J 1989 *J. Phys.: Condens. Matter* **1** 8293
[53] Aoki Y, Nakamichi T and Yamamoto M 1972 *Phys. Stat. Sol. (b)* **53** K137
[54] Fujii H, Pourarian F and Wallace W E 1981 *J. Magn. Magn. Mater.* **24** 93
[55] Wiesinger G, Oppelt A and Buschow K H J 1981 *J. Magn. Magn. Mater.* **22** 227
[56] Muraoka Y, Shiga M and Nakamura Y 1979 *J. Phys. F: Met. Phys.* **9** 1889
[57] Coehoorn R 1989 *Phys. Rev.* B **39** 13072
[58] Vosko S H, Wilk L and Nusair M 1980 *Can. J. Phys.* **58** 1200
[59] Shirakawa K, Ohnuma S, Nose M and Masumoto T 1980 *IEEE Trans. Magn.* **MAG-16** 1129
[60] Friedel J 1963 *Metallic Solid Solutions* ed J Friedel and A Guinier (New York: Benjamin) p 287
[61] Jarlborg T and Peter M 1984 *J. Magn. Magn. Mater.* **42** 89
[62] Blaha P, Schwarz K and Dederichs P H 1988 *Phys. Rev.* B **38** 9368
[63] Moruzzi V L, Janak J F and Williams A R 1978 *Calculated Electronic Properties of Metals* (New York: Pergamon)
[64] Janak J F 1978 *Solid State Commun.* **25** 53
[65] Kanematsu K 1971 *J. Phys. Soc. Japan* **31** 1355
[66] Stobiecki T, Beyreuther G and Hoffmann H 1987 *Proc. Symp. on Magnetic Properties of Amorphous Metals, Benalmadena (Spain)* and reported in [40]
[67] Oshima R, Tanimoto M, Fujita F E, Nose M and Masumoto T 1981 *Rapidly Quenched Metals IV* ed K Suzuki and T Masumoto (Sendai: The Japan Institute of Metals) p 1117
[68] Hosoma T and Nanao S 1981 *Rapidly Quenched Metals IV* ed K Suzuki and T Masumoto (Sendai: The Japan Institute of Metals) p 1125
[69] Turek I 1990 *Hyperfine Interactions* **62** 343
[70] Blügel S, Akai H, Zeller R and Dederichs P H 1987 *Phys. Rev.* B **35** 3271
Sjörström J 1987 *Thesis* Uppsala University
[71] Kübler J, Höck K-H, Sticht J and Williams A R 1988 *J. Appl. Phys.* **63** 3482
[72] Mryasov O N, Liechtenstein A I, Sandratskii L M and Gubanov V A 1991 *J. Phys.: Condens. Matter* **3** 7683
[73] Krey U, Krauss U and Krompiewski S 1992 *J. Magn. Magn. Mater.* **103** 37

[74] Papaconstantopoulos D A 1986 *Handbook of the Band Structure of Elemental Solids* (New York: Plenum)
[75] Kakehashi Y 1990 *Phys. Rev.* B **41** 9207
Kakehashi Y 1991 *Phys. Rev.* B **43** 10820
[76] Wang C S, Klein B M and Krakauer H 1985 *Phys. Rev. Lett.* **54** 1852
[77] Moruzzi V L, Marcus P M and Kübler J 1989 *Phys. Rev.* B **39** 6957
[78] Kübler J 1989 *Solid State Commun.* **72** 631
[79] White R M 1983 *Quantum Theory of Magnetism* (Berlin: Springer) p 142